

Confinement of two-dimensional excitons in a non-homogeneous magnetic field

J. A. K. Freire*, A. Matulis†, and F. M. Peeters‡

Departement Natuurkunde, Universiteit Antwerpen (UIA), Universiteitsplein 1, B-2610 Antwerp, Belgium

V. N. Freire and G. A. Farias

Departamento de Física, Universidade Federal do Ceará, Centro de Ciências Exatas, Campus do Pici, Caixa Postal 6030, 60455-760 Fortaleza, Ceará, Brasil

(October 21, 2019)

The effective Hamiltonian describing the motion of an exciton in an external non-homogeneous magnetic field is derived. The magnetic field plays the role of an effective potential for the exciton motion, results into an increment of the exciton mass and modifies the exciton kinetic energy operator. In contrast to the homogeneous field case, the exciton in a non-homogeneous magnetic field can also be trapped in the low field region and the field gradient increases the exciton confinement. The trapping energy and wave function of the exciton in a GaAs two-dimensional electron gas for specific circular magnetic field configurations are calculated. The results show that excitons can be trapped by non-homogeneous magnetic fields, and that the trapping energy is strongly correlated with the shape and strength of the non-homogeneous magnetic field profile.

71.35.Ji, 75.70.Cn, 71.35.-y

I. INTRODUCTION

Two dimensional confinement of excitons or atoms by magnetic fields is an important phenomenon in physics, and is expected to bring a significant improvement to lasers and other functional devices¹. Numerous works have been carried out on the study of the exciton properties in applied magnetic fields^{2–6}. However, for the most part, all the attention has been focused on the influence of homogenous fields on the exciton inner properties. Several theoretical investigations and experiments show the possibility of trapping and guiding of atoms by means of non-homogeneous magnetic fields^{7,8}. Recently, numerous papers⁹ have appeared on the properties of charged particles, like e. g. electrons, in different non-homogeneous magnetic field profiles. For example, quantum mechanical bound states were found which had no classical analogue. Christianen *et al*^{10,11} performed photoluminescence (PL) measurements on excitons in the presence of non-homogeneous magnetic fields. Strips of ferromagnetic material (see, e.g., Ref.¹²) on top of a quantum well were used to create strong magnetic field gradients. They concluded that excitons are forced to regions of low field gradient and that magnetic traps for excitons are feasible. To the best of our knowledge, there is no theoretical work in the literature on studies of excitons in non-homogeneous magnetic fields.

The purpose of the present paper is to develop a mathematical formalism for calculating the quantum mechanical properties of excitons in a non-homogeneous magnetic field, and to illustrate the trapping possibilities of the excitons in some magnetic field profiles. These ones are created by the deposition of magnetic disks and also superconducting disks on top of a two dimensional electron gas (2DEG) with a homogeneous field applied perpendicular to the 2DEG. It results in a non-homogeneous magnetic dipole type of profile and in a magnetic antidot¹³ profile, respectively, in the 2DEG.

The layout of the paper is as follows. In Sec. II the effective Hamiltonian describing the exciton motion in the non-homogeneous magnetic field is derived. In Sec. III we consider circular symmetric magnetic field profiles and reduce the exciton Hamiltonian to a one-dimensional (1D) Schrödinger equation subjected to a spatially dependent effective potential and effective mass. In Sec. IV we calculate explicitly the magnetic field profiles used in our work and study how strongly they are able to trap excitons. Our numerical results for the exciton trapping energies are discussed in Sec. V, and the conclusions are given in Sec. VI.

II. THE EFFECTIVE HAMILTONIAN

We consider a 2D system of two particles with opposite charge interacting via the Coulomb interaction and moving in a non-homogeneous magnetic field characterized by the vector potential $\mathbf{A}(\mathbf{r})$. The Hamiltonian of that system is given by:

$$H = \frac{\hbar^2}{2m_e} \left\{ -i\nabla_e + \frac{e}{\hbar c} \mathbf{A}(\mathbf{r}_e) \right\}^2 + \frac{\hbar^2}{2m_h} \left\{ -i\nabla_h - \frac{e}{\hbar c} \mathbf{A}(\mathbf{r}_h) \right\}^2 - \frac{e^2}{\varepsilon |\mathbf{r}_e - \mathbf{r}_h|}, \quad (1)$$

where ε is the dielectric constant of the material the exciton is moving in, m_e (m_h) is the electron (hole) effective mass, and \mathbf{r}_e , \mathbf{r}_h are the electron and hole coordinates, respectively, in the xy -plane. To simplify the above Hamiltonian, we use the center of mass $\mathbf{R} = (m_e \mathbf{r}_e + m_h \mathbf{r}_h)/M$ and relative motion coordinates $\mathbf{r} = \mathbf{r}_e - \mathbf{r}_h$, where $M = m_e + m_h$ is the total mass of the exciton. Next, in order to obtain the correct asymptotic behavior, we apply a wave function phase transformation analogous to the one used by Gor'kov and Dzyaloshinsky² in the case of a homogeneous magnetic field:

$$\Psi(\mathbf{R}, \mathbf{r}) \rightarrow \exp \{ -i(e/\hbar c) \mathbf{r} \cdot \mathbf{A}(\mathbf{R}) \} \Psi(\mathbf{R}, \mathbf{r}), \quad (2)$$

which leads to the following transformed Hamiltonian:

$$\begin{aligned} H = & \frac{\hbar^2}{2m_e} \left\{ -i \frac{m_e}{M} \nabla_R - i \nabla_r + \frac{e}{\hbar c} \mathbf{A} \left(\mathbf{R} + \frac{m_h}{M} \mathbf{r} \right) - \frac{em_e}{\hbar c M} \nabla_R \{ \mathbf{r} \mathbf{A}(\mathbf{R}) \} - \frac{e}{\hbar c} \mathbf{A}(\mathbf{R}) \right\}^2 \\ & + \frac{\hbar^2}{2m_h} \left\{ -i \frac{m_h}{M} \nabla_R + i \nabla_r - \frac{e}{\hbar c} \mathbf{A} \left(\mathbf{R} - \frac{m_e}{M} \mathbf{r} \right) - \frac{em_h}{\hbar c M} \nabla_R \{ \mathbf{r} \mathbf{A}(\mathbf{R}) \} + \frac{e}{\hbar c} \mathbf{A}(\mathbf{R}) \right\}^2 \\ & - \frac{e^2}{\varepsilon r}. \end{aligned} \quad (3)$$

In real experimental situations^{9,11} the size of the exciton is smaller than the length scale over which the magnetic field varies, which allows us to use the adiabatic approach⁴. We assume that the exciton relative motion is fast as compared with its center-of-mass motion, and that the characteristic dimension in the relative coordinate (i.e. the exciton radius) is much smaller than that of the center-of-mass motion (i.e. the characteristic length of the magnetic field inhomogeneity). This allows us to expand the vector potential $\mathbf{A}(\mathbf{R} \pm m_{h(e)} \mathbf{r}/M)$ into \mathbf{r} power series restricting the consideration with up to second order terms. Note that the exciton radius in GaAs, e.g., is typically $a_B^* = \varepsilon \hbar^2 / \mu e^2 \simeq 120 \text{ \AA}$, while the magnetic field inhomogeneity varies typically on a micron scale^{11,12,14}. Within the adiabatic approximation, we obtain the following expression for the exciton Hamiltonian:

$$H = \frac{\hbar^2}{2\mu} \left(-i \nabla_r + \xi \frac{e}{\hbar c} \{ (\mathbf{r} \cdot \nabla_R) \mathbf{A}(\mathbf{R}) \} \right)^2 + \frac{\hbar^2}{2M} \left(i \nabla_R + \frac{e}{\hbar c} [\mathbf{r} \times \mathbf{B}(\mathbf{R})] \right)^2 - \frac{e^2}{\varepsilon r}, \quad (4)$$

where $\mu = m_e m_h / M$ is the exciton reduced mass and $\xi = (m_h - m_e) / M$. The first term in the Hamiltonian, (Eq. 4), describes the kinetic energy of the exciton relative motion, in which the expression $\xi(\mathbf{r} \cdot \nabla_R) \mathbf{A}(\mathbf{R})$ can be interpreted as an effective vector potential describing the local magnetic field $\xi \mathbf{B}(\mathbf{R})$. We can choose the gauge such that $(\mathbf{r} \cdot \nabla_R) \mathbf{A}(\mathbf{R}) = \mathbf{B}(\mathbf{R}) \times \mathbf{r} / 2 + \nabla_r \{ (\mathbf{r} \cdot \nabla_R) \{ \mathbf{r} \cdot \mathbf{A}(\mathbf{R}) \} \} / 2$, and simplify the second term of this expression by applying the following transformation:

$$\Psi(\mathbf{R}, \mathbf{r}) \rightarrow \exp \{ -i\xi(e/\hbar c) \Omega(r) \} \Psi(\mathbf{R}, \mathbf{r}), \quad (5)$$

with $\Omega(r) = (\mathbf{r} \cdot \nabla_R) \{ \mathbf{r} \cdot \mathbf{A}(\mathbf{R}) \} / 2$. The above transformation does not change the center-of-mass motion, and leads only to the appearance of r^3 -order terms in the relative motion, which are neglected in the present adiabatic approach. In doing so, we obtain the following transformed Hamiltonian:

$$H = -\frac{\hbar^2}{2\mu} \nabla_r^2 - \frac{e^2}{\varepsilon r} + W_1 + W_2 - \frac{\hbar^2}{2M} \nabla_R^2, \quad (6)$$

where terms of first and second power in the magnetic field strength are denoted by

$$\begin{aligned} W_1 &= \frac{e}{2c\mu} \xi \mathbf{B}(\mathbf{R}) \cdot \mathbf{L} + \frac{ie\hbar}{2Mc} \{ \mathbf{B}(\mathbf{R}) \times \nabla_R - \nabla_R \times \mathbf{B}(\mathbf{R}) \} \cdot \mathbf{r}, \\ W_2 &= \frac{e^2}{8c^2\mu} B(\mathbf{R})^2 r^2. \end{aligned} \quad (7)$$

Here the symbol $\mathbf{L} = \{ \mathbf{r} \times (-i\hbar \nabla_r) \}$ stands for the exciton relative angular momentum operator. Notice that in case of a homogeneous magnetic field the above Hamiltonian reduces to the one which can be found in the literature (see Ref. 5 and references therein). The exciton Hamiltonian in a homogeneous magnetic field consists of a part with no magnetic field dependence, a part linear (the angular momentum term) in the magnetic field, and a quadratic part

(the diamagnetic shift term) in the magnetic field. In the present Hamiltonian which describes the exciton motion in a non-homogeneous magnetic field we also have these terms, but now they are position dependent. We also have an additional term with a linear dependence in the magnetic field (the last term in the W_1 Hamiltonian, Eq. (7)) which results from the gradient in the magnetic field, and which modifies the exciton mass.

Now within the spirit of the above adiabatic approach, the total exciton wave function is represented as the product of the wave functions describing its relative and center-of-mass motions, i. e., $\Psi(\mathbf{R}, \mathbf{r}) = \Phi(\mathbf{r})\psi(\mathbf{R})$. Next, it is supposed that the relative motion wave function $\Phi(\mathbf{r})$ obeys the Schrödinger equation with the Hamiltonian H^{rel} which includes all terms of total Hamiltonian, Eq. (6), except the last one describing the kinetic energy of the center-of-mass motion:

$$\{H^{rel} - E(\mathbf{R}, \nabla_R)\} \Phi(\mathbf{r}) = 0. \quad (8)$$

Note that in contrary to the standard adiabatic approach¹⁵ the relative motion Hamiltonian (see Eq. (7)) depends not only on the center-of-motion coordinate \mathbf{R} but also on the gradient ∇_R . It does not complicate, however, the effective Hamiltonian derivation, but one should take into account that now the eigenvalue of the relative motion equation, which usually plays a role of the effective potential for the center-of-mass equation, is an operator and gives the correction to the kinetic center-of-mass operator as well. So, the effective center-of-mass Hamiltonian has to be presented as follows

$$H^{CM} = -\frac{\hbar^2}{2M} \nabla_R^2 + E(\mathbf{R}, \nabla_R). \quad (9)$$

We solve the relative motion, Eq. (8), by means of a perturbation technique in magnetic field strength powers restricting our consideration by the second order terms. This assumption is valid in weak field regime ($\hbar\omega_c^* < 2R_y^*$), where $R_y^* = \mu e^4/2\varepsilon^2\hbar^2$ is the effective Rydberg, and $\omega_c^* = eB/\mu c$ is the cyclotron-resonance frequency. This is the magnetic field regime relevant for experiments with non-homogeneous magnetic fields^{14,16,17} which contrasts with experiments in homogeneous magnetic fields where usually the high field regime $\hbar\omega_c^* \gg 2R_y^*$ is reached. Notice that $\hbar\omega_c^* = 2R_y^*$ corresponds to $B \approx 5$ T for GaAs.

Now taking into account the cylindrical symmetry of the zero order Hamiltonian

$$H_0 = -\frac{\hbar^2}{2\mu} \nabla_r^2 - \frac{e^2}{\varepsilon r}, \quad (10)$$

we find the zero order wave function

$$\Phi_0^{n,m}(\mathbf{r}) = A_{n,m} \left(\frac{2\lambda_n r}{a_B^*} \right)^{|m|} \exp \left(im\varphi - \frac{\lambda_n r}{a_B^*} \right) L_{n+|m|-1}^{2|m|} \left(\frac{2\lambda_n r}{a_B^*} \right), \quad (11)$$

corresponding to the zero order eigenvalue

$$E_0(n, m) = -\lambda_n^2 R_y^*, \quad \lambda_n = (n - 1/2)^{-1}, \quad (12)$$

where the symbols n and m stands for the radial and angular relative motion quantum numbers, a_B^* is the effective Bohr radius, $A_{n,m}$ is the normalization constant determined by $\langle \Phi_0^{n,m}(\mathbf{r}) | \Phi_0^{n,m}(\mathbf{r}) \rangle = 1$, and $L_n^{(\alpha)}(x)$ is the generalized Laguerre polynomial¹⁸. Solving in addition the first order equation

$$\{H_0 - E_0(n, m)\} \Phi_1^{n,m}(\mathbf{r}) = \{E_1(n, m) - W_1\} \Phi_0^{n,m}(\mathbf{r}), \quad (13)$$

with the orthogonality condition $\langle \Phi_1^{n,m}(\mathbf{r}) | \Phi_0^{n,m}(\mathbf{r}) \rangle = 0$, we obtain the first and the second eigenvalue corrections

$$E_1(n, m) = \langle \Phi_0^{n,m}(\mathbf{r}) | W_1 | \Phi_0^{n,m}(\mathbf{r}) \rangle = \frac{e\hbar}{2\mu c} \xi B_z(\mathbf{R}) m, \quad (14)$$

$$\begin{aligned} E_2(n, m) &= \langle \Phi_0^{n,m}(\mathbf{r}) | W_2 | \Phi_0^{n,m}(\mathbf{r}) \rangle + \langle \Phi_0^{n,m}(\mathbf{r}) | [W_1 - E_1(n, m)] | \Phi_1^{n,m}(\mathbf{r}) \rangle \\ &= \beta_m^n \frac{e^2 a_B^{*2}}{8\mu c^2} B_z(\mathbf{R})^2 + \alpha_m^n \frac{e^2 \hbar^2 a_B^{*2}}{2R_y^* M^2 c^2} \nabla_R \{ B_z(\mathbf{R})^2 \nabla_R \}. \end{aligned} \quad (15)$$

Here the symbols α_m^n and β_m^n are numerical constants which follow from the averages in Eq. (15). For a magnetic field perpendicular to the xy -plane we obtained the following values: $\alpha_0^1 = 21/128$, $\beta_0^1 = 3/8$, $\alpha_0^2 = 365/64$, $\beta_0^2 = 35/4$, and $\alpha_{\pm 1}^2 = 145/128$, $\beta_{\pm 1}^2 = 11/4$.

Inserting the obtained eigenvalue corrections into Eq. (9) we obtain the final expression for the effective Hamiltonian

$$H^{CM} = -\frac{\hbar^2}{2M} \nabla_R \left\{ 1 - \alpha_{m_r}^{n_r} \frac{e^2 a_B^{*2}}{Mc^2 R_y^*} B_z(\mathbf{R})^2 \right\} \nabla_R - \lambda_{n_r}^2 R_y^* + \frac{e\hbar}{2\mu c} \xi m_r B_z(\mathbf{R}) + \beta_{m_r}^{n_r} \frac{e^2 a_B^{*2}}{8\mu c^2} B_z(\mathbf{R})^2, \quad (16)$$

which describes the center-of-mass motion of the exciton with relative motion quantum numbers (n_r, m_r) in the non-homogeneous magnetic fields.

III. CYLINDRICAL SYMMETRY

From now on we limit ourselves to cylindrical symmetric magnetic field profiles $B_z(\mathbf{R}) = B_z(R)$. Then, the exciton center-of-mass wave function $\psi(\mathbf{R})$ can be written as:

$$\psi(\mathbf{R}) = \frac{1}{\sqrt{2\pi}} \exp\{im_R\phi\} \psi(R), \quad (17)$$

where m_R is the quantum number corresponding to the exciton center-of-mass angular momentum. Hamiltonian Eq. (16) then leads to the following radial Schrödinger equation:

$$\left\{ -\frac{\hbar^2}{2R} \frac{d}{dR} \left[\frac{R}{M^{eff}(R)} \frac{d}{dR} \right] + V^{eff}(R) - E \right\} \psi(R) = 0, \quad (18)$$

where

$$M^{eff}(R) = \frac{M}{1 - \alpha_{m_r}^{n_r} c_1 B_z(R)^2}, \quad (19)$$

is the effective mass for the center-of-mass motion of the exciton, and

$$V^{eff}(R) = \beta_{m_r}^{n_r} c_2 B_z(R)^2 + m_r c_3 B_z(R) + E_0(n_r, m_r) + \frac{\hbar^2}{2M^{eff}(R)} \frac{m_R^2}{R^2}, \quad (20)$$

is the effective potential for the exciton with

$$c_1 = \frac{e^2 a_B^{*2}}{R_y^* Mc^2} \quad ; \quad c_2 = \frac{e^2 a_B^{*2}}{8\mu c^2} \quad ; \quad c_3 = \frac{e\hbar}{2\mu c} \xi. \quad (21)$$

For GaAs we have typically $a_B^* \simeq 120 \text{ \AA}$, $R_y^* \simeq 5 \text{ meV}$, $c_1 \simeq 6.25 \times 10^{-3} \text{ T}^{-2}$, $c_2 \simeq 0.44 \text{ meV T}^{-2}$ and $c_3 \simeq 0.69 \text{ meV T}^{-1}$. Please note that the 2D exciton ground state energy $E_0(1, 0)$ is $-4R_y^* \simeq -20 \text{ meV}$ and the 2D exciton size is one half the Bohr radius, $a_B^*/2 = 60 \text{ \AA}$. From the above equations, we notice that the non-homogeneous magnetic field modifies the exciton center-of-mass motion in the following ways. First the exciton feels a $B_z(R)^2$ effective potential. It implies that excitons will be collected in a region where the magnetic field strength is minimum. Next, the exciton mass is enhanced, it increases with $B_z(R)^2$, which favours the localization of excitons. Third, the kinetic term gives a contribution proportional to the gradient in the B -field, i.e., a $dB_z(R)/dR$ term. Finally, we see that the non-homogeneous magnetic field also interacts with the exciton angular momentum, and that this interaction is controlled by the difference in mass ξ . The reason is that the exciton is a neutral particle, and if the electron and hole would have the same mass, the angular momentum term would not contribute because, electron and hole give the same contribution but with opposite sign.

IV. MAGNETIC FIELD PROFILES

We solve Eq. (18) numerically using the confinement potential generated by two different non-homogeneous magnetic field profiles, which experimentally are created by the deposition of (a) a magnetized disk and (b) a superconducting disk on top of a 2DEG, with a homogeneous magnetic field (B_a) applied perpendicular to the 2DEG. Such an experimental configuration results in a non-homogeneous magnetic field profile in the 2DEG. The first profile (a) results into a magnetic dipole type of profile, and the second (b) is also called the magnetic antidot¹³. A sketch of the two experimental systems, the magnetized disk and the superconducting disk, are shown in the inset of Fig. 1(b) and Fig. 3(a), respectively.

A. Magnetized Disk

To calculate the magnetic field created by a magnetized disk, we assume that the disk is very thin and is completely magnetized in the z -direction. Therefore, we can write the magnetization in the following way:

$$\mathbf{M}(\mathbf{R}) = h\mathcal{M}\delta(Z - d)\theta(a - R)\mathbf{e}_Z, \quad (22)$$

where h is the disk thickness, a is the disk radius, d the distance of the magnetic disk to the 2DEG, \mathcal{M} the magnetisation, $\theta(a - R)$ is the Heaviside step function, and Z and $R = \sqrt{X^2 + Y^2}$ are cylindrical coordinates. The corresponding vector potential can be calculated from the differential form of Ampéres law $\nabla_R^2 \mathbf{A}(\mathbf{R}) = -4\pi\nabla_R \times \mathbf{M}(\mathbf{R})^{19}$. In cylindrical coordinates, the vector potential has only an angular component:

$$A_\varphi(R) = 4B_0^D \sqrt{\frac{a}{R}} \frac{1}{p} \left\{ -E(p^2) + \left(1 - \frac{p^2}{2}\right) K(p^2) \right\}, \quad (23)$$

with

$$p = 2 \frac{\sqrt{aR}}{\sqrt{(a + R)^2 + d^2}}, \quad (24)$$

where $B_0^D = h\mathcal{M}$, and $K(x)$ ($E(x)$) is the elliptic integral of first (second) type. The magnetic field can be evaluated straightforwardly from $\mathbf{B}(\mathbf{R}) = \nabla \times \mathbf{A}(\mathbf{R})$, which results into:

$$\begin{aligned} B_z(R) &= \frac{(a + R)}{(a + R)^2 + d^2} A_\varphi(R) + B_0^D \frac{(a^2 - R^2 + d^2)}{R^2 \sqrt{aR}} p^3 \\ &\times \left\{ -\frac{\partial}{\partial p^2} E(p^2) - \frac{1}{2} K(p^2) + \left(1 - \frac{p^2}{2}\right) \frac{\partial}{\partial p^2} K(p^2) \right\}. \end{aligned} \quad (25)$$

The magnetic field profile of the magnetized disk (the magnetic dipole profile) in the 2DEG for $d = 0.2 \mu\text{m}$, $a = 2 \mu\text{m}$, and $B_0^D = 0.1 \text{ T}$ is shown in the inset of Fig. 1(a). Due to the quadratic dependence of the effective potential on the magnetic field (see Eq. (22)), we can maximize the confinement potential by applying a homogeneous field B_a to the magnetic dipole profile, $B_z^{total}(R) = B_a + B_z(R)$. We use the experimental results of Dubonos *et al*¹⁶ in order to take values for the applied field (B_a) smaller than the coercivity field, which has a strong dependence with the radius of the magnetized disk¹⁶.

The magnetic dipole profile in the 2DEG for different values of the relation d/a are shown in Fig. 1(a) (Fig. 2(a)) as a function of the radial coordinate, in the presence of a homogeneous magnetic field $B_a = 0.35 \text{ T}$ ($B_a = -0.25 \text{ T}$), where we took $B_0^D = 0.1 \text{ T}$. We also show in Fig. 1 ($B_a = 0.35 \text{ T}$) and in Fig. 2 ($B_a = -0.25 \text{ T}$) the effective potential, Eq. (20), for the exciton center-of-mass motion for the 1s (Fig. 1(a) and Fig. 2(a)), and for the 2p⁻ (Fig. 1(b) and Fig. 2(b)) exciton relative motion quantum state, and the effective mass (Fig. 1(b) and Fig. 2(b)), Eq. (19), for the 2p⁻ exciton relative motion quantum state.

Notice that the effective potential, Figs. 1-2, is negative. This is due to the energy shift resulting from the zero field exciton relative motion $E_0(n_r, m_r)$ in the equation of the effective potential (see Eq. (20)). This energy increases with increasing principal relative motion quantum number n_r (see Eq. (12)). Also notice that the effective potential of the excited levels of the exciton relative motion (e.g., see Fig. 1-2(b) for the 2p⁻ state) has a confinement region larger than the 1s relative quantum level. The reason for this is as follows: the coefficient of the diamagnetic term in the effective potential equation (the term with quadratic dependence in the magnetic field in Eq. (20)), $\beta_{m_r}^{n_r}$, is related to the averaging of r^2 in the wave function of the exciton relative motion, i.e., $\beta_{m_r}^{n_r} \propto \langle \Phi_0^{n_r, m_r}(\mathbf{r}) | r^2 | \Phi_0^{n_r, m_r}(\mathbf{r}) \rangle$ (see Eq. (15)) which increases for increasing n_r . Then, the confinement for the n_r exciton relative motion states should be stronger than the one for the $n_r - 1$ relative state. Further, the exciton angular momentum term in the exciton Hamiltonian is, in practice, bigger than the diamagnetic term. This is because the effective potential for the exciton relative motion quantum states with $m_r \neq 0$ has confinement energies larger than the one for the relative levels with $m_r = 0$ (compare, e.g., the energy range in Fig. 1(a) and Fig. 1(b)).

The last term in our effective potential, Eq. (20), is related to the angular momentum of the exciton center-of-mass motion, m_R . In that case, it contributes to the potential like a centrifugal term (m_R/R^2), and leads to a peak near $R = 0$ (see dotted curve in Fig. 1-2(b)). Also notice that the effective mass is position dependent (see dashed curve in Fig. 1-2(b)). It is larger than the normal exciton mass $M = 0.407$ although its increase is small.

B. Superconducting Disk

The magnetic antidot was recently discussed by Reijniers *et al*¹³, where the properties of electrons in a two dimensional system confined by such a magnetic antidot were investigated. They found that, the magnetic field profile below a very thin type-I superconducting disk is given by:

$$B_z(R) = B_a \left\{ 1 + \frac{2}{\pi} \left[\frac{a\zeta}{(a^2 + \zeta^2)} - \arctan \left(\frac{a}{\zeta} \right) \right] \right\} + \frac{2B_a}{\pi} \frac{a\zeta(a^2 - \eta^2)}{(a^2 + \zeta^2)(\zeta^2 + \eta^2)}, \quad (26)$$

with

$$\begin{aligned} \zeta^2 &= \frac{1}{2} \left[\sqrt{(R^2 + d^2 - a^2)^2 + 4a^2d^2} + (R^2 + d^2 - a^2) \right], \\ \eta^2 &= \frac{1}{2} \left[\sqrt{(R^2 + d^2 - a^2)^2 + 4a^2d^2} - (R^2 + d^2 - a^2) \right], \end{aligned} \quad (27)$$

where a is the disk radius, and d the distance of the superconducting disk to the 2DEG. In Fig. 3(a) the magnetic field profile resulting from the superconducting disk (magnetic antidot), and the effective potential, Eq. (20), for the 1s exciton relative motion quantum state is shown for $a = 0.3 \mu\text{m}$ and for $d/a = 0.1$ (dashed and dashed-dot curves) and $d/a = 0.01$ (solid and dotted curves). The effective mass, Eq. (19), and the effective potential for the 2p⁻ exciton relative motion quantum state is plotted in Fig. 3(b) for $d/a = 0.1$. We took in Fig. 3(a) (Fig. 3(b)) an applied magnetic field B_a of 2 T (1 T). Notice that the magnetic field in the 2DEG is suppressed below the superconducting disk and an overshoot is found near the edge of the disk which becomes smoother with increasing distance, d , between the superconducting disk and the 2DEG. The exciton will prefer to localize below the disk because V^{eff} is smaller there. This is no longer true for the 2p⁻ state (see Fig. 3(b)) where now V^{eff} has a local minimum near the edge of the disk where the magnetic field exhibits the largest gradient. This occurs when the applied field B_a is such that the diamagnetic term (quadratic in the magnetic field) in the effective potential, Eq. (20), becomes comparable to the angular momentum term (linear in the magnetic field).

V. NUMERICAL RESULTS FOR THE EXCITON TRAPPING ENERGY

We have calculated the trapping energy and wave functions of an exciton in a GaAs 2DEG in the presence of the above non-homogeneous magnetic field profiles (magnetic dipole and magnetic antidot profiles). The electron and hole mass and the dielectric constant used in our calculations are⁴ $m_e = 0.067m_0$, $m_h = 0.34m_0$, and $\varepsilon = 12.53$, respectively. The problem of finding the eigenfunctions and energies of Eq. (18) was solved by using a similar numerical discretization technique as was used in Ref. 20.

We define the exciton trapping energy as the difference between the exciton energy in the homogeneous applied field B_a and the energy of the exciton in the non-homogeneous magnetic field profile for the same exciton state. Following this definition, a positive exciton trapping energy implies that the exciton is trapped in the effective potential created by the field inhomogeneity. The influence of all the terms in Eqs. (21) and (22) on the exciton trapping are extensively discussed. The possibility of exciton trapping by using the confinement potential created by the magnetic dipole, Figs. 1-2, and the magnetic antidot, Fig. 3, are analyzed. In all the following figures, if not explicitly stated otherwise, the disk radius and the distance to the 2DEG used for the magnetized disk and for the superconducting disk are $a = 2 \mu\text{m}$, and $a = 0.3 \mu\text{m}$, respectively, and we took the distance to the 2DEG equal to $d = 0.1a$.

The trapping energy for the ground state of the exciton, for the center-of-mass quantum numbers $(n_R, m_R) = (1,0)$ (dashed curves) and $(1,1)$ (triangles) are shown in Fig. 4 for the magnetic dipole profile with a homogeneous applied field of (a) $B_a = 0.35 \text{ T}$ and (b) $B_a = -0.25 \text{ T}$ as a function of the magnetisation of the disk B_0^D . Similar results are shown in Fig. 5 for the magnetic antidot profile as a function of the applied magnetic field B_a . Notice that for both profiles in low fields, the trapping energy is negative (i.e., unbound state), indicating that a large part of the center-of-mass exciton wave function is extended into the magnetic barrier region. The $(n_R, m_R) = (1,1)$ is an excited state and requires slightly larger magnetic fields to become bound. With increasing magnetic field the exciton becomes more and more confined which increases the trapping energy E_B . The magnetic disk in the presence of a negative applied field (Fig. 4(b)) has a critical field where the trapping energy starts to decrease with increasing field. This is due to the competition between the magnetic field generated by the disk B_0^D , and the applied field B_a . When the field of the disk increases, the center region of the corresponding effective potential (see solid curve in Fig. 2(a)) which has a peak structure can become comparable to V^{eff} at the edge of the disk which for large B_0^D (e.g. for $(n_R, m_R) = (1,0)$ in Fig. 4(b) this occurs for $B_0^D > 0.06 \text{ T}$) may lead to a complete vanishing of the confinement

region. One can increase the trapping energy by applying a stronger homogeneous field B_a , which is not trivial due to the limited coercivity field and for sufficient large B_a it will flip the magnetisation of the disk and we end up into the situation of Fig. 1(a).

The angular momentum interaction with the magnetic field is responsible for important effects in the trapping of atoms by non-homogeneous magnetic fields⁷. In two-dimensional exciton systems, the momentum-field interaction is of importance in a variety of exciton properties. The exciton trapping energies for the seven lowest levels of the center-of-mass motion, for the (a) $2p^-$, (b) $2s$, and (c) $2p^+$, exciton relative motion quantum states are shown in Fig. 6 (Fig. 7) for the magnetic dipole profile with $B_a = 0.35$ T ($B_a = -0.25$ T) as a function of B_0^D , and in Fig. 8 for the magnetic antidot as a function of B_a . In the case of the magnetic dipole profile, the exciton in the $2p^\pm$ states are much more confined than the $2s$ state. The reason is that the angular momentum term in Eq. (20) gives a confinement potential stronger than the diamagnetic term. Notice that in the case of a negative applied field, due to this strong confinement of the $2p^\pm$ states (Fig. 7), only the $2s$ state is affected by the competition between the fields B_0^D and B_a as was discussed for Fig. 3. The trapping energy of the superconducting disk profile also increases with increasing magnetic field but for the $2p^-$ exciton relative motion quantum state (Fig. 8(a)) there is a local maximum in the trapping energy. This energy starts to decrease after some field ($B_a = 1$ T in Fig. 8(a)), which is exactly when the quadratic term (positive) begins to be comparable to the angular momentum term (negative) in Eq. (20) (see effective potential in Fig. 3(b)).

Also notice that the exciton center-of-mass quantum levels with non zero angular momentum ($m_R \neq 0$) have only slightly higher energy than the levels with $m_R = 0$. The reason is because the $m_R = 0$ term in the effective potential, Eq. (20), only is responsible for a very small peak near $R = 0$ which gives a very small contribution to the total effective potential. The trapping energy in Figs. 6-8 are typically two orders of magnitude larger than the one for the $1s$ state of the exciton relative motion. In general, the trapping energy corresponding to the n_r exciton relative quantum state resulting from the magnetic field inhomogeneity should be bigger than the one corresponding to the $n_r - 1$ quantum state. This can be easily understood from the effective potential equation, Eq. (20). The coefficient of the diamagnetic term, $\beta_{m_r}^{n_r}$, increases with increasing n_r which increases the exciton trapping energy.

Figs. 9(a,b) and Fig. 10 show the ground-state radial wave function of the exciton center-of-mass motion (see Eq. (18)) for the magnetic dipole profile for $B_a = 0.35$ T and $B_a = -0.25$ T, and for the superconducting disk, respectively, as a function of the radial coordinate R , for the quantum numbers of the relative motion $(n_r, m_r) = (1,0)$, for different values of B_0^D (magnetized disk) and B_a (superconducting disk). Notice that with increasing magnetic field the exciton becomes more localized. The wave functions in Figs. 9(b) and 10 correspond to the effective potential profiles of Figs. 2(a) and Fig. 3(a) which have the minimum of the potential near the center of the disk, and that is where the exciton is localized. In contrast to the case of Fig. 9(a) the effective potential (see Fig. 1(a)) has its minimum near the outer edge of the disk where the exciton becomes localized. In the latter case the center-of-mass wave function will have a ring like structure.

In order to investigate the dependence of the exciton trapping energy on the size of the magnetic field inhomogeneity, we calculated the trapping energy for the $2s$ exciton relative motion quantum state (i.e., $(n_r, m_r) = (2,0)$), as a function of the disk radius a . The results are shown in Figs. 11(a,b) for the magnetic dipole profile with $B_0^D = 0.05$ T and a homogeneous field of $B_a = 0.35$ T and $B_a = -0.25$ T, respectively, and in Fig. 12 for the magnetic antidot profile with $B_0 = 0.5$ T, in each case for the seven lowest quantum numbers of the center-of-mass motion. In Fig. 11 (Fig. 12) we took the distance to the 2DEG $d = 0.2 \mu\text{m}$ ($0.03 \mu\text{m}$). The trapping energy increases with disk radius but it saturates for large a . The reason is that for sufficient large a only the width of the potential minimum increases but no longer the depth and consequently the trapping energy becomes equal to the depth of the minimum in V^{eff} .

VI. CONCLUSIONS

In conclusion, we have developed a formalism to describe the exciton motion in a two dimensional system, in the presence of a non-homogeneous magnetic field. We assumed that the length scale for the variation of the magnetic field is large as compared to the exciton radius. We have theoretically calculated the exciton trapping energies for the non-homogeneous magnetic fields created by a magnetized disk (the magnetic dipole type profile) and by a superconducting disk (the magnetic antidot). The results show that the trapping energy has a significant dependence on the radius and profile of the non-homogeneous magnetic field, as well as on the homogeneous applied background magnetic field B_a . Further, the exciton angular momentum interaction with the non-homogeneous magnetic field can be responsible for shifts as big as a factor of 10 in comparison with the states with zero angular momentum. In the present analysis we neglected the spin of the electron and the hole which may have an important effect on the trapping energy when the effective g -factor is substantially different from zero. The analysis of the latter will be left for future research.

ACKNOWLEDGMENTS

This work was supported by the Inter-university Micro-Electronics Center (IMEC, Leuven), the Flemish Science Foundation (FWO-VI), and IUAP (Belgium). J. A. K. Freire was supported by the Brazilian Ministry of Culture and Education (MEC-CAPES) and F. M. Peeters is a research director with the FWO-VI. We acknowledge stimulating discussions with F. Pullizzi

* Permanent address: Departamento de Física, Universidade Federal do Ceará, Centro de Ciências Exatas, Campus do Pici, Caixa Postal 6030, 60455-760 Fortaleza, Ceará, Brasil.

† Permanent address: Semiconductor Physics Institute, Goštauto 11, 2600 Vilnius, Lithuania.

‡ Electronic address: peeters@uia.ua.ac.be

¹ M. -O. Mewes, M. R. Andrews, N. J. van Druten, D. M. Kurn, D. S. Durfee, and W. Ketterle, Phys. Rev. Lett. **77**, 416 (1997).

² L. P. Gor'kov and I. E. Dzyaloshinsky, Sov. Phys. JETP **26**, 449 (1968).

³ I. V. Lerner and Yu. E. Lozovik, Sov. Phys. JETP **51**, 588 (1980).

⁴ N. R. Cooper and D. B. Chklovskii, Phys. Rev. B **55**, 2436 (1996).

⁵ A. B. Dzyubenko, JETP Lett. **66**, 617 (1997).

⁶ V. D. Kulakovskii, JETP Lett. **66**, 286 (1997).

⁷ W. Petrich, M. H. Anderson, J. R. Ensher, and E. A. Cornell, Phys. Rev. Lett. **74**, 3352 (1995).

⁸ J. J. Tollett, C. C. Bradley, C. A. Sackett, and R. G. Hulet, Phys. Rev. A **51**, R22 (1995).

⁹ For a recent review see: F. M. Peeters and J. De Boeck, in *Handbook of nanostructured materials and nanotechnology*, edited by H. S. Nalwa (Academic Press, New York, 1999), Vol. 3, p. 345.

¹⁰ P. C. M. Christianen, F. Piazza, J. G. S. Lok, J. C. Maan, and W. van der Vleuten, Physica B **249-251**, 624 (1998).

¹¹ F. Pulizzi, P. C. M. Christianen, J. C. Maan, T. Wojtowicz, G. Karczewski, and J. Kossut, OECS6 (Ascona, 1999), to be published in Phys. Status Solidi A.

¹² A. K. Geim, S. V. Dubonos, J. G. S. Lok, I. V. Grigorieva, J. C. Maan, L. Theil Hansen, and P. E. Lindelof, Appl. Phys. Lett. **71**, 2379 (1997).

¹³ J. Reijnders, A. Matulis, and F. M. Peeters, Phys. Rev. B **59**, 2817 (1999).

¹⁴ A. K. Geim, I. V. Grigorieva, S. V. Dubonos, J. G. S. Lok, J. C. Maan, A. E. Lindelof, and F. M. Peeters, Nature **390**, 259 (1997).

¹⁵ M. Born and Kun Huang, *Dynamical theory of crystal lattices*, (Oxford: Clarendon Press, 1968). Wednesday, October 20, 1999 at 15:48

¹⁶ S. V. Dubonos, A. K. Geim, K. S. Novoselov, J. G. S. Lok, J. C. Maan, and M. Henini, EP2DS-13 (Ottawa, 1999), to be published in Physica E.

¹⁷ V. Kubrak, F. Rahman, B. L. Gallagher, P. C. Main, M. Henini, C. H. Marrows, and M. A. Howson, Appl. Phys. Lett. **74**, 2507 (1999).

¹⁸ *Handbook of Mathematical Functions*, M. Abramowitz and I. A. Stegun, (Dover Publications, New York, 1972), p. 775.

¹⁹ *Classical Electrodynamics*, J. D. Jackson (John Wiley & Sons, New York, 1962), p. 153.

²⁰ F. M. Peeters and V.A. Schweigert, Phys. Rev. B **53**, 1468 (1995).

FIG. 1. (a) Effective potential for $m_R = 0$ and $(n_r, m_r) = (1,0)$ and the magnetic field profile $B(R)$ of the magnetized disk (inset of figure magnetic field profile in the 2DEG in the absence of a background field) with a positive homogeneous applied field $B_a = 0.35$ T, as a function of the radial coordinate R , for $d/a = 0.1$ with $V^{eff}(R)$ (solid) and $B(R)$ (dotted), and $d/a = 0.2$ with $V^{eff}(R)$ (dashed-dotted) and $B(R)$ (dashed). (b) Effective potential $V^{eff}(R)$ for $n_r = 2$, $m_r = -1$ with: i) $m_R = 0$ (solid) with corresponding effective mass $M^{eff}(R)$ (dashed), and ii) $V^{eff}(R)$ for $m_R = 1$ (dotted) as a function of R , for $d/a = 0.1$. We took $B_0^D = 0.1$ T and the disk radius $a = 2.0 \mu\text{m}$.

FIG. 2. (a) Effective potential for $m_R = 0$ and $(n_r, m_r) = (1,0)$ and the magnetic field profile $B(R)$ of the magnetized disk with a negative homogeneous applied field $B_a = -0.25$ T, as a function of the radial coordinate R , for $d/a = 0.1$ with $V^{eff}(R)$ (solid) and $B(R)$ (dotted), and $d/a = 0.2$ with $V^{eff}(R)$ (dashed-dotted) and $B(R)$ (dashed). (b) Effective potential $V^{eff}(R)$ for $n_r = 2$, $m_r = -1$ with: i) $m_R = 0$ (solid) with corresponding effective mass $M^{eff}(R)$ (dashed), and ii) $V^{eff}(R)$ for $m_R = 1$ (dotted) as a function of R , for $d/a = 0.1$. We took $B_0^D = 0.1$ T and the radius $a = 2.0 \mu\text{m}$.

FIG. 3. (a) Effective potential $V^{eff}(R)$ for $m_R = 0$, $(n_r, m_r) = (1,0)$ and corresponding magnetic field profile $B(R)$ of the superconducting disk, as a function of the radial coordinate R , for $d/a = 0.1$ with $V^{eff}(R)$ (dashed-dot) and $B(R)$ (dashed), and $d/a = 0.01$ with $V^{eff}(R)$ (solid) and $B(R)$ (dotted), and (b) effective potential $V^{eff}(R)$ for $n_r = 2$, $m_r = -1$, $m_R = 0$ (solid) with corresponding effective mass $M^{eff}(R)$ (dashed), and $V^{eff}(R)$ for $m_R = 1$ (dotted), as a function of R , for $d/a = 0.1$. We took the radius $a = 0.3 \mu\text{m}$ and an applied field B_0 of (a) 2 T and (b) 1 T.

FIG. 4. Exciton trapping energy, E_B , for $(n_R, m_R) = (1,0)$ (dashed curve) and $(1,1)$ (triangles), and $(n_r, m_r) = (1,0)$, for the magnetic dipole profile as a function of B_0^D , for (a) $B_a = 0.35$ T and (b) $B_a = -0.25$ T, and for $a = 2 \mu\text{m}$ and $d/a = 0.1$.

FIG. 5. Exciton trapping energy, E_B , for $(n_R, m_R) = (1,0)$ (dashed curve) and $(1,1)$ (triangles), and $(n_r, m_r) = (1,0)$, for the magnetic antidot profile as a function of B_a , and for $d/a = 0.1$, with $a = 0.3 \mu\text{m}$.

FIG. 6. Exciton trapping energy, E_B , as a function of B_0^D , for the magnetic dipole profile for a homogeneous applied field $B_a = 0.35$ T, for $a = 2 \mu\text{m}$ and $d/a = 0.1$, and for $n_r = 2$, and (a) $m_r = -1$, (b) $m_r = 0$, and (c) $m_r = +1$. The different curves correspond to the different exciton center-of-mass levels $(n_R, m_R) = (1,0)$ dashed curve, $(1,1)$ triangles, $(2,0)$ dotted curve, $(2,1)$ squares, $(3,0)$ solid curve, $(3,1)$ circles, and $(4,0)$ dashed-dotted curve.

FIG. 7. The same as in Fig. 6 but now for the magnetic dipole profile with a homogeneous applied field of $B_a = -0.25$ T.

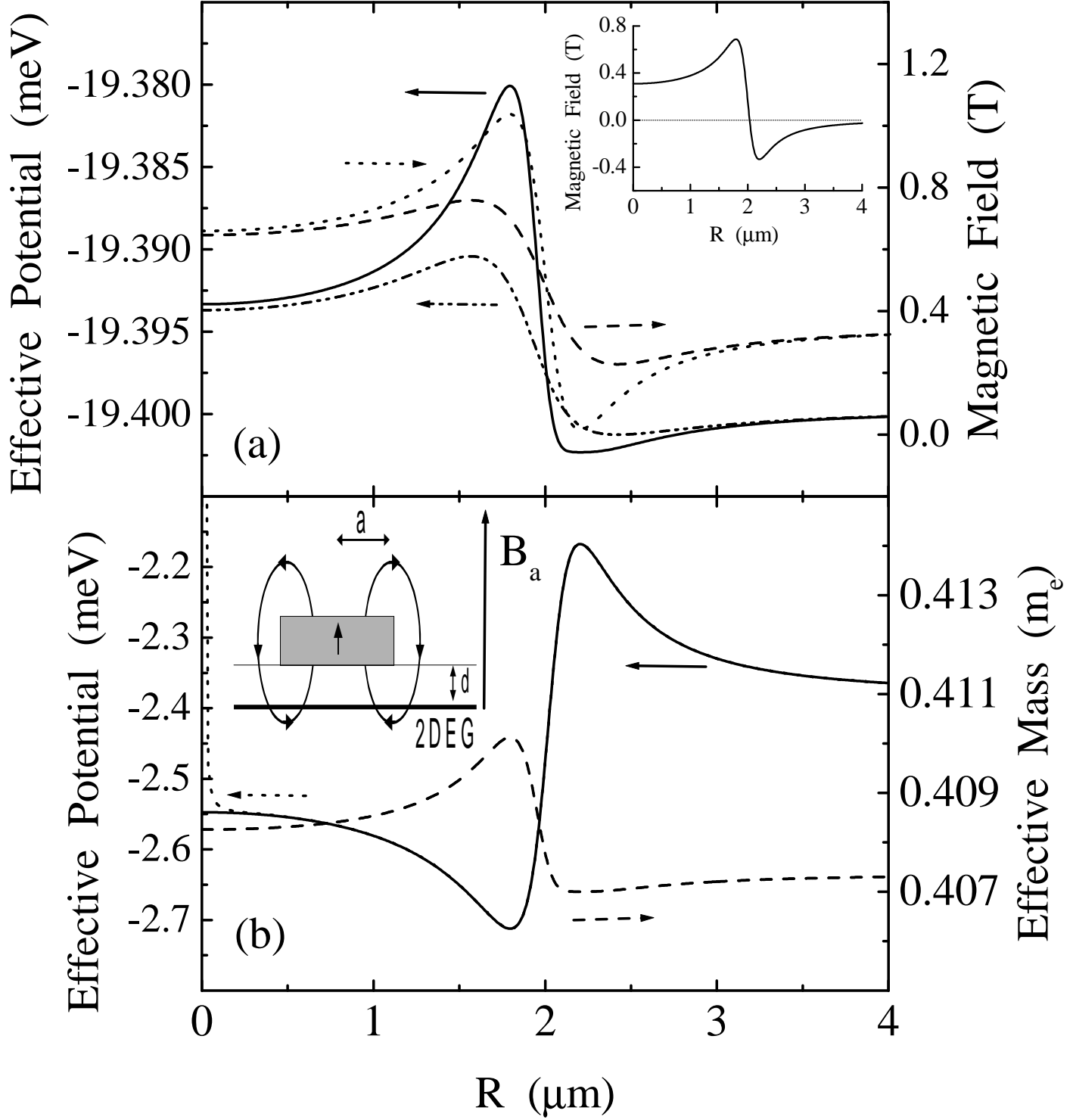
FIG. 8. The same as in Fig. 6 but now as a function of B_a , for the magnetic antidot profile, for $a = 0.3 \mu\text{m}$ and $d/a = 0.1$.

FIG. 9. Exciton center-of-mass radial wave function $\psi(R)$ as a function of the radial coordinate R , for the magnetic dipole profile, for (a) $B_a = 0.35$ T and (b) $B_a = -0.25$ T, for $(n_R, m_R) = (1,0)$, $(n_r, m_r) = (1,0)$, for $a = 2 \mu\text{m}$ and $d/a = 0.1$, and for $B_0^D = 0.02$ T (dotted), 0.06 T (solid), and 0.1 T (dashed).

FIG. 10. The same as in Fig. 9(a) but now for the magnetic antidot profile, and for $a = 0.3 \mu\text{m}$ and $d/a = 0.1$, and for $B_a = 1$ T (dotted), 1.5 T (solid), and 2.0 T (dashed).

FIG. 11. Exciton trapping energy, E_B , for $(n_r, m_r) = (2,0)$, as a function of the disk radius a , for the magnetic dipole profile for (a) $B_a = 0.35$ T and (b) $B_a = -0.25$ T, for $d = 0.2 \mu\text{m}$ and $B_0^D = 0.05$ T, and for center-of-mass quantum numbers $(n_R, m_R) = (1,0)$ dashed curve, $(1,1)$ triangles, $(2,0)$ dotted curve, $(2,1)$ squares, $(3,0)$ solid curve, $(3,1)$ circles, and $(4,0)$ dashed-dotted curve.

FIG. 12. The same as in Fig. 11(a) but now for the magnetic antidot profile, and for $d = 0.03 \mu\text{m}$ and $B_a = 0.5$ T.



Effective Potential (meV)

(a)

0.6

0.3

0.0

-0.3

-0.6

Magnetic Field (T)

Effective Potential (meV)

(b)

0.4082

0.4078

0.4074

0.4070

Effective Mass (m_e)

Effective Potential (meV)

0 1 2 3 4

R (μm)

